Propagation characteristics of power line harmonic radiation in the ionosphere*

Wu Jing(吴 静)†, Fu Jing-Jing(付静静), and Zhang Chong(张 翀)

School of Automation Science and Electrical Engineering, Beihang University, Beijing 100191, *China*

(Received 26 August 2013; revised manuscript received 22 September 2013; published online 12 February 2014)

Theoretical model and solutions on power line harmonic radiation (PLHR) propagating in the ground, air, and anisotropic homogeneous ionosphere are presented. The theoretical model is verified by the PLHR events observed by the DEMETER satellite. Some propagation characteristics of PLHR based on the model are obtained. This paper is beneficial to quantitatively interpret the formation mechanism of PLHR phenomenon.

Keywords: power line harmonic radiation, anisotropic medium, ionosphere, electromagnetic waves

PACS: 41.20.Jb, 52.40.Db, 92.60.Ta **DOI:** 10.1088/1674-1056/23/3/034102

1. Introduction

Harmonics in the high voltage power system not only affect the power quality, do harm to the normal operation of the power grid and disturb the communication system on the ground, but also pollute the ionosphere and magnetosphere via power line harmonic radiation (PLHR).[1–7] The PLHR can stimulate nonlinear wave–particle and wave–wave interactions in the magnetosphere, result in wave growth and energetic electron precipitation, trigger new emissions, and significantly affect natural radio noise. The main sources of PLHR are transmission line corona discharge (up to 10 MHz), gas discharge, and nonlinear terminal loads. The frequency interval of PLHR is 50 or 60 Hz which is the working frequency of power grid.

As an anthropogenic pollution to the space environment,[1] the ground-based observations, the space-based detections, numerical simulations, and physical experiments on the PLHR have attracted more attention.[2] About the formation mechanism of PLHR, Carson analyzed the wave propagation in horizontal long straight wire with the ground return.[8] Ni used an analytic method to calculate the load responses of the two-wire transmission line excited by a plane wave.[9] Wedepohl presented the wave propagation model in transmission lines over the lossy ground.[10] Yearby measured the PLHR power radiating into the magnetosphere at harmonics from 60 Hz up to 4500 Hz.[3] Tatnall studied the generation and radiation of power line harmonics considered as long-wire aerial.[4] Kikuchi described the wave propagation along an infinite transmission line above the ground.[11] However, there have been so far proposed by very few articles of theoretical analysis on the PLHR in the presence of the ionosphere. Only Ando analyzed the penetration characteristics of PLHR into ionosphere theoretically in 2002.[5]

The physical model of PLHR propagated in the Earth, atmosphere, and the anisotropic homogeneous ionosphere is discussed in this paper. Section 2 presents the physical model and its solutions. They are verified by the PLHR events observed by DEMETER satellite in Section 3. We also analyze the propagation characteristics of the PLHR in the ionosphere. Finally, the conclusions are drawn in Section 4.

2. Physical model of the PLHR and its solutions

The physical model of PLHR is shown in Fig. 1. Assume that the interfaces between the Earth, atmosphere, and the ionosphere are infinite planes. The geomagnetic field B_0 is directed along the $+z$ direction. An infinitely long and thin wire carrying current $i(t) = I\cos(\omega t)$ is located at $z = z_0$, and its density is $\boldsymbol{J} = \delta(x)\delta(z-z_0)I\cos(\omega t)\,\boldsymbol{e}_y$, where $\delta(x)$ stands for the Dirac's function. The time harmonic factor is $\mathrm{e}^{-\mathrm{j}\omega t}$ and ω is the angular frequency.

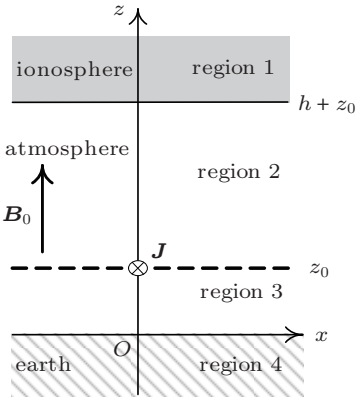


Fig. 1. Physical model of the PLHR.

*Project supported by the National Natural Science Foundation of China (Grant No. 51207006) and the Natural Science Foundation of Beijing, China (Grant No. 3123038).

†Corresponding author. E-mail: wujing06@buaa.edu.cn

© 2014 Chinese Physical Society and IOP Publishing Ltd

Region 1 is the ionosphere where $z > h + z_0$. It is regarded as lossless and uniformly magnetized cold plasma with the permittivity tensor

$$\varepsilon_{\boldsymbol{r}} = \varepsilon_0 \begin{bmatrix} \kappa_1 & -\mathrm{j}\kappa_2 & 0 \\ \mathrm{j}\kappa_2 & \kappa_1 & 0 \\ 0 & 0 & \kappa_3 \end{bmatrix}, \tag{1}$$

where

$$\kappa_1 = 1 - \sum_j \frac{\omega_{\mathrm{p}j}^2}{\omega^2 - \omega_{\mathrm{c}j}^2}, \quad \kappa_2 = \sum_j \frac{\omega_{\mathrm{c}j}\omega_{\mathrm{p}j}^2}{\omega(\omega^2 - \omega_{\mathrm{c}j}^2)},$$
$$\kappa_3 = 1 - \sum_j \frac{\omega_{\mathrm{p}j}^2}{\omega^2}.$$

Here, $\omega_{\mathrm{p}j}$ and $\omega_{\mathrm{c}j}$ are the plasma frequency and cyclotron frequency of the particle species j and given, respectively, by

$$\omega_{\mathrm{p}j} = \sqrt{N_j (Z_j e)^2 / m_j \varepsilon_0}, \quad \omega_{\mathrm{c}j} = -(Z_j e / m_j) B_0,$$

where N_j is the particle density, $Z_j e$ is the charge, and m_j is the quality.

The atmosphere includes both region 2 ($z_0 < z < z_0 + h$) and region 3 ($0 < z < z_0$). They are interfaced by the infinite long wire. The dielectric constant and magnetic permeability of the air are ε_0 and μ_0, respectively. Region 4 ($z < 0$) is the Earth which is taken as a semi-infinite perfect conductor.

Based on the physical model, the field we discuss is two-dimensional.

2.1. Constraint equations and boundary conditions

The Maxwell equations in region i ($i = 1, 2, 3, 4$) are

$$\nabla \times \boldsymbol{H}_i = \frac{\partial \boldsymbol{D}_i}{\partial t}, \tag{2}$$
$$\nabla \times \boldsymbol{E}_i = -\frac{\partial \boldsymbol{B}_i}{\partial t}, \tag{3}$$
$$\nabla \cdot \boldsymbol{D}_i = 0, \tag{4}$$
$$\nabla \cdot \boldsymbol{B}_i = 0. \tag{5}$$

To make these equations easier to be solved, we transform them into wave number domain by Fourier transform as

$$\tilde{f}(k) = \frac{1}{2\pi} \int_{-\infty}^{+\infty} f(x) \mathrm{e}^{-\mathrm{j}kx} \mathrm{d}x, \tag{6}$$
$$f(x) = \int_{-\infty}^{+\infty} \tilde{f}(k) \mathrm{e}^{\mathrm{j}kx} \mathrm{d}k, \tag{7}$$

where $f(x)$ stands for the field variable in time domain, and $\tilde{f}$ is in the wave number domain.

In region 1, the medium parameters satisfy $\boldsymbol{D}_1 = \bar{\varepsilon}_r \cdot \boldsymbol{E}_1$ and $\boldsymbol{B}_1 = \mu_o \boldsymbol{H}_1$. In regions 2 and 3, $\boldsymbol{D}_i = \varepsilon_0 \cdot \boldsymbol{E}_i$ and $\boldsymbol{B}_i = \mu_o \boldsymbol{H}_i$ ($i = 2, 3$).

The interface conditions are defined as follows:

$$\begin{cases} \tilde{H}_{1x} - \tilde{H}_{2x} = 0, \\ \tilde{H}_{1y} - \tilde{H}_{2y} = 0, \\ \tilde{E}_{1x} - \tilde{E}_{2x} = 0, \\ \tilde{E}_{1y} - \tilde{E}_{2y} = 0, \end{cases} \quad \text{at } z = h + z_0, \tag{8}$$

$$\begin{cases} \tilde{H}_{2x} - \tilde{H}_{3x} = \dfrac{I}{2\pi}, \\ \tilde{H}_{2y} - \tilde{H}_{3y} = 0, \\ \tilde{E}_{2x} - \tilde{E}_{3x} = 0, \\ \tilde{E}_{2y} - \tilde{E}_{3y} = 0, \end{cases} \quad \text{at } z = z_0, \tag{9}$$

$$\begin{cases} \tilde{H}_{3x} - \tilde{H}_{4x} = 0, \\ \tilde{H}_{3y} - \tilde{H}_{4y} = 0, \\ \tilde{E}_{3x} - \tilde{E}_{4x} = 0, \\ \tilde{E}_{3y} - \tilde{E}_{4y} = 0, \end{cases} \quad \text{at } z = 0. \tag{10}$$

2.2. Analytical solutions

Solving the boundary value problems in Section 2.1, we obtain the solutions in region 1 as

$$\begin{aligned} \tilde{\boldsymbol{E}}_1 = & -\frac{1}{k}(S_1 A \mathrm{e}^{\mathrm{j}\gamma_1 z} + \mathrm{j} S_2 Z B \mathrm{e}^{\mathrm{j}\gamma_2 z}) \boldsymbol{e}_x \\ & + \frac{\omega\mu_0}{k}(-\mathrm{j} Y A \mathrm{e}^{\mathrm{j}\gamma_1 z} + B \mathrm{e}^{\mathrm{j}\gamma_2 z}) \boldsymbol{e}_y \\ & + (A \mathrm{e}^{\mathrm{j}\gamma_1 z} + \mathrm{j} Z B \mathrm{e}^{\mathrm{j}\gamma_2 z}) \boldsymbol{e}_z, \end{aligned} \tag{11}$$

$$\begin{aligned} \tilde{\boldsymbol{H}}_1 = & \frac{\mathrm{j}}{k}(\gamma_1 Y A \mathrm{e}^{\mathrm{j}\gamma_1 z} + \mathrm{j}\gamma_2 B \mathrm{e}^{\mathrm{j}\gamma_2 z}) \boldsymbol{e}_x \\ & - \frac{\omega\varepsilon_0\kappa_3}{k}(A \mathrm{e}^{\mathrm{j}\gamma_1 z} + \mathrm{j} Z B \mathrm{e}^{\mathrm{j}\gamma_2 z}) \boldsymbol{e}_y \\ & + (-\mathrm{j} Y A \mathrm{e}^{\mathrm{j}\gamma_1 z} + B \mathrm{e}^{\mathrm{j}\gamma_2 z}) \boldsymbol{e}_z, \end{aligned} \tag{12}$$

where

$$\gamma_1^2 = \kappa_1 k_0^2 - \frac{1}{2}\left(1 + \frac{\kappa_1}{\kappa_3}\right)k^2 + \sqrt{w(k)}, \quad \mathrm{Im}(\gamma_1) \geq 0,$$
$$\gamma_2^2 = \kappa_1 k_0^2 - \frac{1}{2}\left(1 + \frac{\kappa_1}{\kappa_3}\right)k^2 - \sqrt{w(k)}, \quad \mathrm{Im}(\gamma_2) \geq 0,$$
$$\begin{aligned} w(k) = & \left\{\kappa_1 k_0^2 - \frac{1}{2}\left(1 + \frac{\kappa_1}{\kappa_3}\right)k^2\right\}^2 \\ & - \frac{\kappa_1}{\kappa_3}(k_0^2\kappa_r - k^2)(k_0^2\kappa_3 - k^2), \end{aligned}$$
$$A = -\frac{kI}{2\pi}\frac{U_2 \sin\gamma_0 z_0 \mathrm{e}^{-\mathrm{j}\gamma_1(z_0+h)}}{D_0 \cos\gamma_0(z_0+h)},$$
$$B = -\frac{kI}{2\pi}\frac{\mathrm{j}Z^{-1}U_1 \sin\gamma_0 z_0 \mathrm{e}^{-\mathrm{j}\gamma_2(z_0+h)}}{D_0 \cos\gamma_0(z_0+h)},$$
$$Y = \frac{\kappa_3\gamma_1^2 - \kappa_1(k_0^2\kappa_3 - k^2)}{\omega\mu_0\kappa_2\gamma_1},$$
$$Z = \frac{\omega\mu_0\kappa_2\gamma_2}{\kappa_3\gamma_2^2 - \kappa_1(k_0^2\kappa_3 - k^2)},$$
$$D_0 = YV_1U_2 - Z^{-1}V_2U_1,$$
$$U_1 = -S_1 + \mathrm{j}\gamma_0\kappa_3 \tan\gamma_0(z_0+h),$$
$$U_2 = -S_2 + \mathrm{j}\gamma_0\kappa_3 \tan\gamma_0(z_0+h),$$
$$V_1 = \gamma_0 - \mathrm{j}\gamma_1 \tan\gamma_0(z_0+h),$$
$$V_2 = \gamma_0 - \mathrm{j}\gamma_2 \tan\gamma_0(z_0+h),$$
$$S_1 = \frac{\kappa_3 k_0^2 - k^2}{\gamma_1}, \quad S_2 = \frac{\kappa_3 k_0^2 - k^2}{\gamma_2}, \quad \gamma_0^2 = k_0^2 - k^2.$$

The electric field strength and the magnetic field strength in region 2 are

$$\tilde{\boldsymbol{E}}_2 = -\frac{\mathrm{j}\gamma_0}{k} C \sin\gamma_0 z \boldsymbol{e}_x + \frac{\omega\mu_0}{k}(D\mathrm{e}^{\mathrm{j}\gamma_0 z} + F\mathrm{e}^{-\mathrm{j}\gamma_0 z}) \boldsymbol{e}_y$$

$$+C\cos\gamma_0 z\boldsymbol{e}_z, \tag{13}$$

$$\tilde{\boldsymbol{H}}_2 = \frac{\gamma_0}{k}(-D\mathrm{e}^{\mathrm{j}\gamma_0 z}+F\mathrm{e}^{-\mathrm{j}\gamma_0 z})\boldsymbol{e}_x - \frac{\omega\varepsilon_0}{k}C\cos\gamma_0 z\boldsymbol{e}_y+(D\mathrm{e}^{\mathrm{j}\gamma_0 z}+F\mathrm{e}^{-\mathrm{j}\gamma_0 z})\boldsymbol{e}_z, \tag{14}$$

where

$$C = -\frac{kI}{2\pi}\frac{\kappa_3(S_1-S_2)\sin\gamma_0 z_0}{D_0\cos^2\gamma_0(z_0+h)},$$

$$D = \frac{\mathrm{j}kI}{4\pi\gamma_0}\frac{\sin\gamma_0 z_0\mathrm{e}^{-\mathrm{j}\gamma_0(z_0+h)}}{D_0\cos\gamma_0(z_0+h)} \times\{(\gamma_0+\gamma_1)YU_2-(\gamma_0+\gamma_2)Z^{-1}U_1\},$$

$$F = \frac{\mathrm{j}kI}{4\pi\gamma_0}\frac{\sin\gamma_0 z_0\mathrm{e}^{\mathrm{j}\gamma_0(z_0+h)}}{D_0\cos\gamma_0(z_0+h)} \times\{(\gamma_0-\gamma_1)YU_2-(\gamma_0-\gamma_2)Z^{-1}U_1\}.$$

The electromagnetic field solutions in the region 3 are

$$\tilde{\boldsymbol{E}}_3 = -\frac{\mathrm{j}\gamma_0}{k}C\sin\gamma_0 z\boldsymbol{e}_x+\frac{\omega\mu_0}{k}G\sin\gamma_0 z\boldsymbol{e}_y +C\cos\gamma_0 z\boldsymbol{e}_z, \tag{15}$$

$$\tilde{H}_3 = \frac{\mathrm{j}\gamma_0}{k}G\cos\gamma_0 z\boldsymbol{e}_x-\frac{\omega\varepsilon_0}{k}C\cos\gamma_0 z\boldsymbol{e}_y +G\sin\gamma_0 z\boldsymbol{e}_z, \tag{16}$$

where

$$G = \frac{\mathrm{j}kI}{2\pi\gamma_0} \times\frac{(YU_2-Z^{-1}U_1)\gamma_0\cos\gamma_0 h-\mathrm{j}(\gamma_1 YU_2-\gamma_2 Z^{-1}U_1)\sin\gamma_0 h}{D_0\cos\gamma_0(z_0+h)}.$$

In region 4, the electromagnetic field in the Earth is $\boldsymbol{E}_4=\boldsymbol{H}_4=0$.

The above formulas defining the electric field strength and the magnetic field strength are in the domain of wave number, and the electromagnetic fields in the spatial domain are obtained by the inverse Fourier transform.

It is noted that the model and solutions in this paper are similar to that of Ref. [5], but equations (13)–(16) in this paper are different from Eqs. (10a), (10b), and (11) in Ref. [5]. The coefficient expressions (A4), (A7), and (A8) of Eq. (10a) and (11) in Ref. [5] are incorrect.

3. Numerical results and verification

3.1. Verification of the physical model and its solutions

Many PLHR events have been detected by space-based measurements. In order to verify the model and its solutions in Section 2, the PLHR events observed by the DEMETER satellite are used. Reference [7] presented a PLHR event recorded on 25 March 2006, when the DEMETER was flying over Finland from 19:13:32 UT (Universal Time) to 19:13:50 UT.

In order to compare with the satellite observation results, the parameters of the physical model are taken as follows.

(i) $z_0 = 30$ m. The height of high voltage power line in Finland is generally 24–32 m.

(ii) $(\boldsymbol{h}+z_0) = 80$ km. The height of the lower boundary of the ionosphere is 80 km according to the international reference ionosphere (IRI).

(iii) The height of the observation point is 672 km, which is the height of DEMETER in the interval shown in Fig. 2.

(iv) According to the measurement data from DEMETER at that time when the PLHR event occurred, the average electron density is 7.6768×10^9 m^{-3}, the average density of the oxygen ions O^+ is 4.3462×10^9 m^{-3}, the average density of the hydrogen ions H^+ is 7.46×10^7 m^{-3}, and the average density of the helium ions He^+ is 4.50×10^7 m^{-3}. The magnetic flux density of geomagnetic field in the z direction is -3.9×10^{-5} T.

(v) The maximum permissible harmonic current at 1750 Hz is 0.06–2.3 A (RMS) in terms of the limits of harmonic current in IEC61000-3-2 and G5/4, the current at 1850 Hz is 0.06–2.3 A (RMS), and the current at 1950 Hz is 0.05–0.4 A (RMS).

The electric field strength and magnetic flux density defined by Eqs. (11) and (12) are compared with the measurement results from the DEMETER in Table 1.

Table 1. Comparison between the results of analysis solutions and those measured by the DEMETER.

f/Hz	I/A	$\lvert E\rvert$/μV·m^{-1}		$\lvert B\rvert/10^{-5}$ nT	
		Analysis	Measurement	Analysis	Measurement
1750	0.06–2.3	0.034–1.274	0.452	0.198–7.613	5.298
1850	0.06–2.1	0.074–2.560	0.294	0.424–14.868	4.612
1950	0.06–0.4	0.059–0.395	0.243	0.335–2.235	3.971

From Table 1, the electric field strengths of the PLHR event detected by satellite are in the range of calculation results from the physical model. The interferences on the measured magnetic field on the DEMETER board are stronger than that on the measured electric field, and the errors of the measured results are greater for higher frequency. Therefore, the measured result of the magnetic field at 1950 Hz is out of the calculated range.

Additionally, the electromagnetic field should be stronger than the background noise in the ionosphere so that it can

be identified by the satellite. The background electric field strength in the ionosphere in 1500–3000 Hz is 0.15 μV/m from the DEMETER data, the region illuminated by the PLHR from the numerical results is within 200 km, while the region of PLHR events observed by the DEMETER is 192 km. They are in a relatively good agreement.

3.2. Propagation characteristics of the PLHR

The dependence of electric field strength and magnetic flux density on frequency f, horizontal distance x, and height z are analyzed. The input parameters of the model are the same as that in Ref. [5]: $z_0 = 10$ m, $h = 80$ km, $I = 1$ A, and $B_0 = 5 \times 10^{-5}$ T, and the density of electrons and ions (mainly O^+) in the ionosphere is $N_e = N_i = 2 \times 10^{11}$ m^{-3}.

Figure 2 shows the numerical results of the electric field strength and magnetic flux density varying with frequency at $x = 0$ km and $z = 600$ km.

As shown in Fig. 2, at higher frequency, the intensity of the electromagnetic field penetrating the ionosphere is higher. There are some peaks of $|E|$ and $|B|$ at 1875, 3749, 5622, and 7497 Hz. These peak frequencies can be obtained from

$$f_{cn} = \frac{nc}{2(z_0 + h)}, \quad n = 0, 1, \ldots,$$

where c is the light speed, and $(z_0 + h)$ is the ionosphere height. These peak frequencies correspond to the cut off frequencies of the Earth–ionosphere waveguide.

Figure 3 shows the electric field strength and magnetic flux density in the ionosphere at 1850 Hz, and figure 4 shows the fields at 3800 Hz.

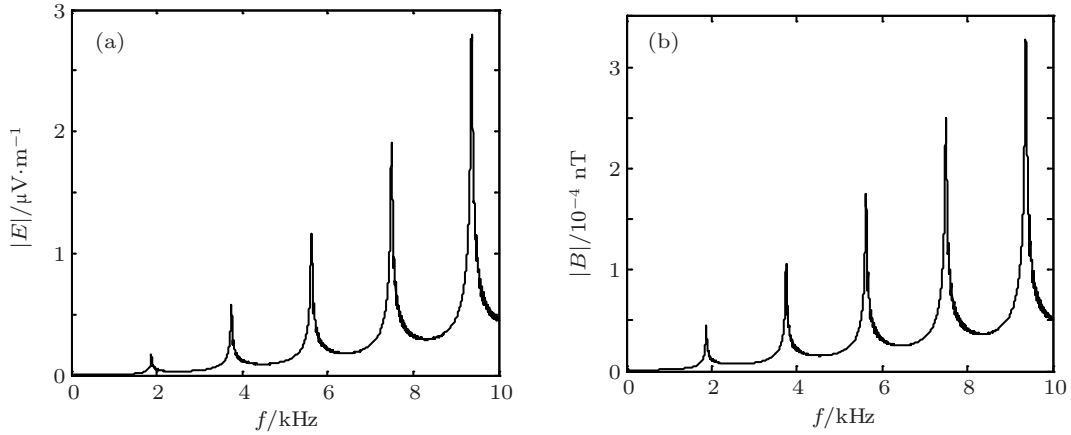


Fig. 2. (a) $|E|$ and (b) $|B|$ versus frequency at $x = 0$ km and $z = 600$ km.

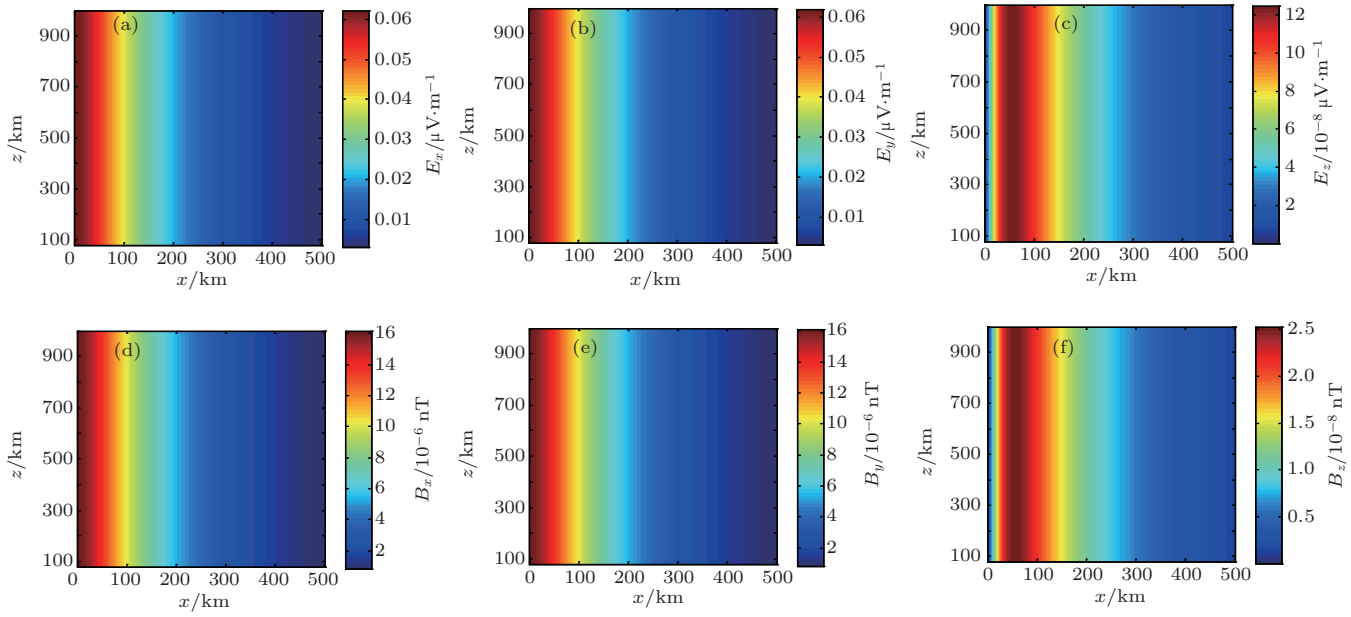


Fig. 3. (color online) (a) $|E_x|$, (b) $|E_y|$, (c) $|E_z|$, (d) $|B_x|$, (e) $|B_y|$, and (f) $|B_z|$ at 1850 Hz in the ionosphere.

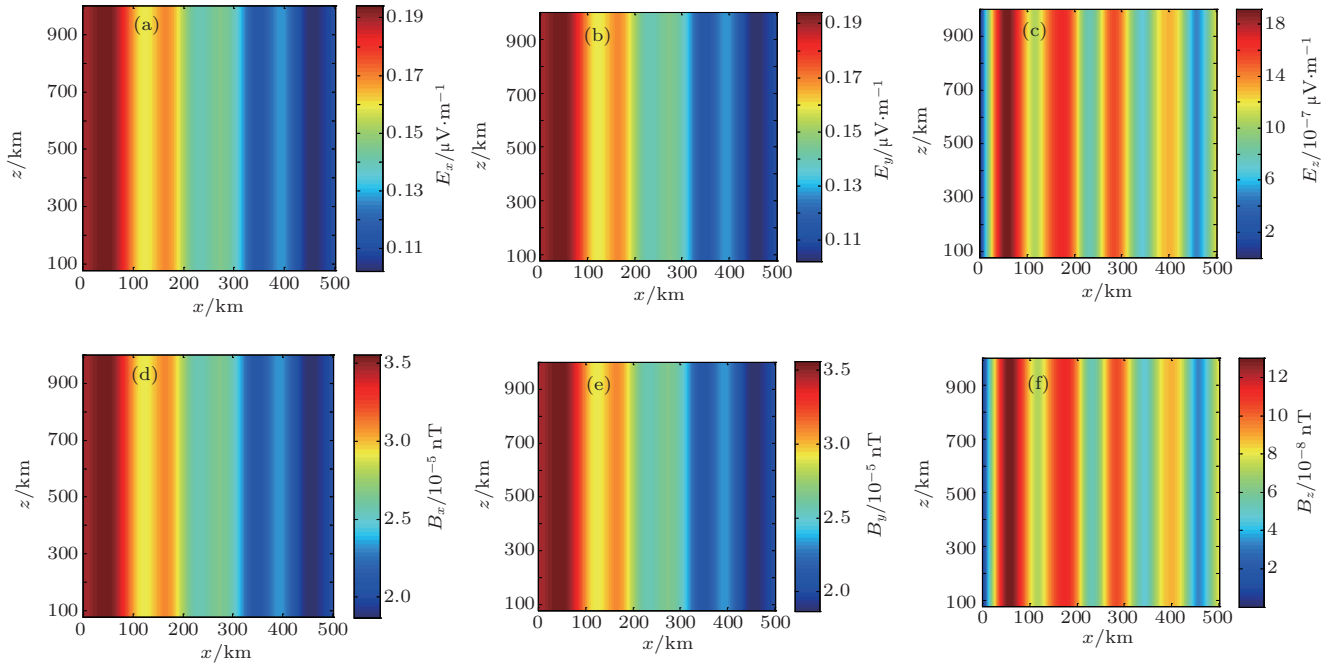


Fig. 4. (color online) (a) $|E_x|$, (b) $|E_y|$, (c) $|E_z|$, (d) $|B_x|$, (e) $|B_y|$, and (f) $|B_z|$ at 3800 Hz in the ionosphere.

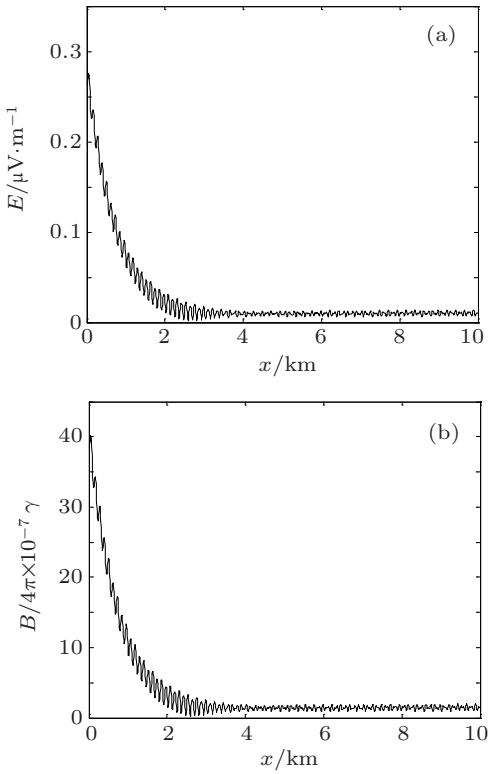


Fig. 5. Distribution of (a) the electric field strength and (b) magnetic flux density at 3800 Hz.

From Figs. 3 and 4, some propagation characteristics of the PLHR are obtained. (i) the vertical components of electric field and magnetic field are negligible compared with the horizontal components, which suggests that the wave vector is nearly along the z direction. (ii) The amplitude of the fields scarcely decays with the increase in altitude. (iii) The fields decrease with increasing horizontal distance in Fig. 3, while the fields in Fig. 4 fluctuate with the increase in horizontal distance. This is due to the poles in the integrands of the spectral integrals (11) and (12) above the lower cutoff frequencies of guided waves of dominant. The poles correspond to the guided wave modes.

In order to estimate the region that the PLHR affects, the field distribution up to $x = 10$ Mm at 3800 Hz is calculated. Figure 5 indicates that there exists a guided wave at 3800 Hz.

4. Conclusions

In this paper, the physical model and solutions of power line harmonic radiation propagating in the ground, atmosphere, and the anisotropic homogenous ionosphere are presented. Theoretical results are verified by the PLHR events detected by the DEMETER satellite. Some propagation characteristics of PLHR are obtained below.

The PLHR propagates in the way of right-hand circular polarization in the ionosphere when the frequency is above the ion cyclotron frequency and below the electron cyclotron frequency, which is different from Ref. [5] that the electric field is elliptically polarized. The polarization direction changes at the cyclotron frequency.

The vertical components of electromagnetic field can be neglected, which suggests that the wave vector is nearly along the z direction.

The amplitude of the fields decrease with the increase in horizontal distance below the lower cutoff frequencies of guided waves of dominant, and fluctuates with the increase in

horizontal distance above the lower cutoff frequencies, which is different from Ref. [5] that the magnetic field intensity monotonically decreases with the increase in horizontal distance above the lower cutoff frequency.

The electric field strength increases with the geomagnetic field, while the magnetic field strength decreases with the geomagnetic field.

References

[1] Bullough K 1995 *Handbook of Atmospheric Electrodynamics* (Vol. 2) (Boca Raton: Fla CRC Press) p. 291

[2] Wu J and Fu J 2011 *Acta Seismol. Sin.* **33** 828 (in Chinese)

[3] Yearby K H, Smith A J, Kaiser T R and Bullough K 1983 *J. Atmos. Terr. Phys.* **45** 409

[4] Tatnall A R L, Matthews J P, Bullouth K and Kaiser T R 1983 *Space Sci. Rev.* **35** 139

[5] Ando Y and Hayakawa M 2002 *Radio Sci.* **37** 1093

[6] Bullough K, Tatnall A R L and Denby M 1976 *Nature* **260** 401

[7] Nemec F, Santolik O, Parrot M and Berthelier J J 2007 *J. Geophys. Res.* **112** A04301

[8] Carson J R 1926 *Bell Syst. Technol. J.* **5** 539

[9] Ni G Y, Yan L and Yuan N C 2008 *Chin. Phys. B* **17** 3629

[10] Wedepohl L M and Efthymiadis A E 1978 *Proc. IEEE* **125** 505

[11] Kikuchi H 1983 *Space Sci. Rev.* **35** 59